Benchmarks for computing induced currents in the human body by ELF electric and magnetic fields

Jean-Pierre Ducreux, Yves Guillot, Pierre Thomas, Noël Burais, Riccardo Scorretti

Benchmarks for computing induced currents in the human body by ELF electric and magnetic fields

Jean-Pierre Ducreux*, Yves Guillot* Pierre Thomas*, Noel Burais**, Riccardo Scorretti **
* LAMEL- EDF R&D, 1 avenue du Général de Gaulle, 92141 Clamart, France
**CNRS, UMR5005, Laboratoire Ampère, Ecully, F-69134, France; Université de Lyon, Lyon, F-69361, France.
Université Lyon 1, Villeurbanne, F-69622, France.

ABSTRACT
Numerical dosimetry is widely used to demonstrate compliancy to regulation. There are several possible approaches but whatever the method is, an appreciation of the numerical imperfections is required. We propose here a geometrical criterion on the finite element mesh. We used an academic benchmark to demonstrate the efficiency and the sensitivity of numerical methods to this criterion.

KEYWORDS

Biological Effects – Electromagnetic Fields – Numerical Dosimetry.

1. INTRODUCTION

Numerical dosimetry of induced electromagnetic fields in the human body is widely used to demonstrate the compliance to regulation, in particular to directive 2004/40/CE [1]. In the extremely frequency (ELF) band, the problem has been solved mainly by using specific formulations which take into account the specific properties of "materials" composing the living tissues [2,3,4,7,8,9]. and notably:

i) wave propagation phenomena are negligible,
ii) displacement currents into the human body are negligible (compared to conduction currents),
iii) the perturbation on the "source" magnetic flux density B due to the induced currents into the human body is negligible: therefore it can be computed in absence of the human body, which is a major simplification of the original problem,
iv) when computing the electric field E outside the human body, this latter can be approximated by a perfect conductor.

The resulting simplified equations have been solved by using mostly Finite Difference methods and Impedance Method (IM). In [2] Dimbylow compute the induced fields by a uniform flux density B by using the Scalar Potential Finite Difference (SPFD) method on the realistic computational phantom of an adult man NORMAN (resolution = 2 mm). The results were compared with those obtained by the same author with the IM, and a very good agreement is found. It is also found that the resolution of the model has a major effect on the obtained value of the maximum value of the induced current density: the higher is the resolution, the higher is the maximum value computed. In [10] Gandhi et al. compute the induced currents by uniform and non uniform radiating ELF sources by using the IM. Compared do SPFD, the IM has the advantage that the magnetic flux density B can be used directly as source term; on the other hand, the number of unknowns is roughly three times bigger. In [11] the induced currents J and electric fields E dues to different configurations of high-voltage transmission lines are computed by SPFD, with a computational phantom of a resolution of 3.6 mm. Different postures of the phantom are taken into account. The results obtained with IM and SPFD methods, and with different computational phantoms have been compared in a cross laboratory study [7]; the main source of discrepancy between the results appears to be the intrinsic differences between the different phantoms used for the computations. The use of temporal schemes like Time Domain Finite Difference (FDTD) is also possible by using the frequency scaling technique [12]. More recently the Finite Integration Technique (FIT) has been used by Bachanski [13, 14]. In these works, a subgriding scheme is used to refine the accuracy of the computation in the most interesting parts of the body. In [4, 15, 16] the Finite Element methods (FEM) has been used by using a phantom composed of tetrahedral elements. The advantage of FEM compared to other methods is its capability to represent complex shapes with a reduced number of geometrical primitives (and hence with less degrees of freedom), and with a flexible refinement (the interesting parts of the body can be meshed with a higher accuracy with respect of uninteresting parts). On the other hand, the task to build the meshed phantom is cumbersome, which explains why FEM are not widely used in numerical dosimetry of ELF EMF.

When dealing with numerical dosimetry it is important to establish on one hand the *reliability* of the computational code, and on the other hand the *accuracy* of the computational phantom. In this work, we focus on the first aspect (reliability of computational codes).
As far as we know no systematic comparison between these methods have been performed using the same benchmarks. Some simulations with a single human model have shown a large variation of results (see companion paper "Impact of current density post-processing for human body exposure to magnetic fields"). Many parameters can explain this variation of results : the geometry, the computational method, the discretization, the post processing …
Thus all these approaches rely on a spatial discretization called a mesh. Numerically the result accuracy is always linked to the mesh fineness. However the fineness is also synonymous of a lot of computation time. So both factors must be balanced. Besides the mesh quality definition depends a lot on the computational technique.

In order to estimate the influence of mesh quality on computed results, we chose to work on an academic benchmark. For this study there exists an analytical expression for induced current density maximum. Some finite element codes have been tested with this benchmark.
This paper is organized in the following way: after a short presentation of the benchmark, we show some results obtained with different tools and methods using the same mesh. We use a coarse and a fine mesh, and we present the results obtained with and without filtering "bad elements" (in the sense which is defined in next sections) away in the post-processing. Finally, these results are discussed.

2. BENCHMARK ANALYSIS

The proposed benchmark consists in several analytical and numerical test-cases, which provide a basis for the validation and inter-comparison of computational codes. These test-cases have been chosen so as to reproduce one particular features of living tissues : low conductivity materials with high permittivity at low frequencies and permeability equal to the one of the void.
We chose conductive spheroids (σ = 0.2 S/m) in a uniform magnetic field varying sinusoidally in time (B eff. = 500 μT along spheroid axis). In cylindrical coordinates, the analytical expression of induced current density modulus maximum J is given by $J = 2\,\sigma\,\pi\,f\,B\,a\,b^2 / (a^2 + b^2)$ where σ is the conductivity, f the frequency, 2a and 2b are the minor and major axes of the ellipse perpendicular to the induction axis (cf. Figure 1).

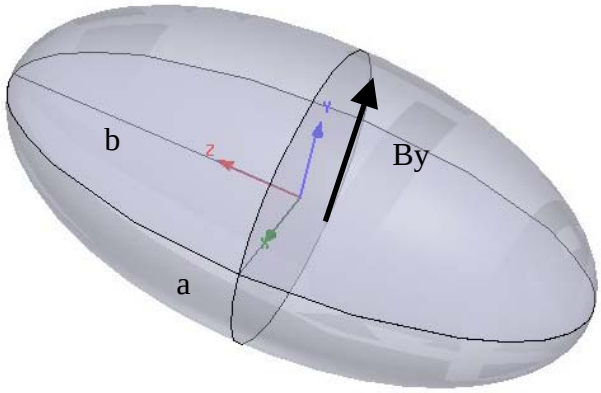

Figure 1 : Description of the ellipsoid – Definition of major axis (b) and minor axis (a) in case of flux source along y -axis

3. MESH ANALYSIS

Some approaches to appreciate mesh quality are proposed in [6]. We chose here to analyse the mesh quality with a geometrical criterion. For each tetrahedron, two particular spheres can be defined. The first one is the insphere that is tangent to the faces. The second one is the circumscribed sphere that touches each tetrahedron's vertice. In Figure 2, in case of a very flattened tetrahedron (right), the largest sphere is the circumscribed sphere and the gray one is the insphere.

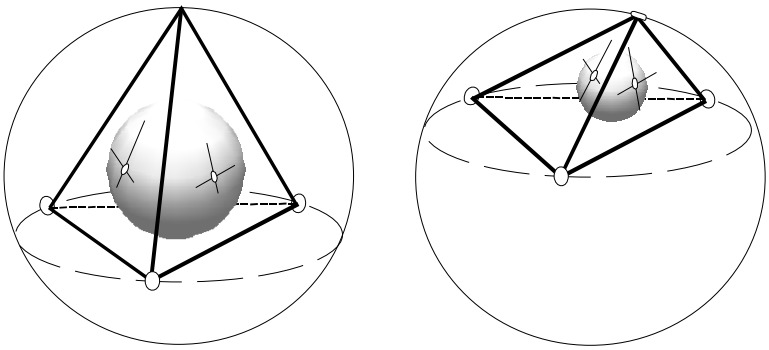

Figure 2 : Representation of circumscribed sphere and insphere

The ratio between the radius of the first sphere and the radius of the second one is chosen here as a criterion of mesh quality. It means that post–processing will be only performed on tetrahedral elements with a good criterion (less than 10%)

4. RESULTS

For several spheroid sizes as in [5], we computed current density with a coarse mesh and a fine mesh (cf. Figure 3). The aim of the computation is to calculate the maximum of the current density inside the spheroid. The same Finite Element meshes are used for each software.
Thus for one software, discrepancies can only be explained by mesh refinement. Depending on the formulation (A-V, T-Ω [17] or φ-A [4,18]), the numerically computed current density is more or less sensitive to mesh quality.

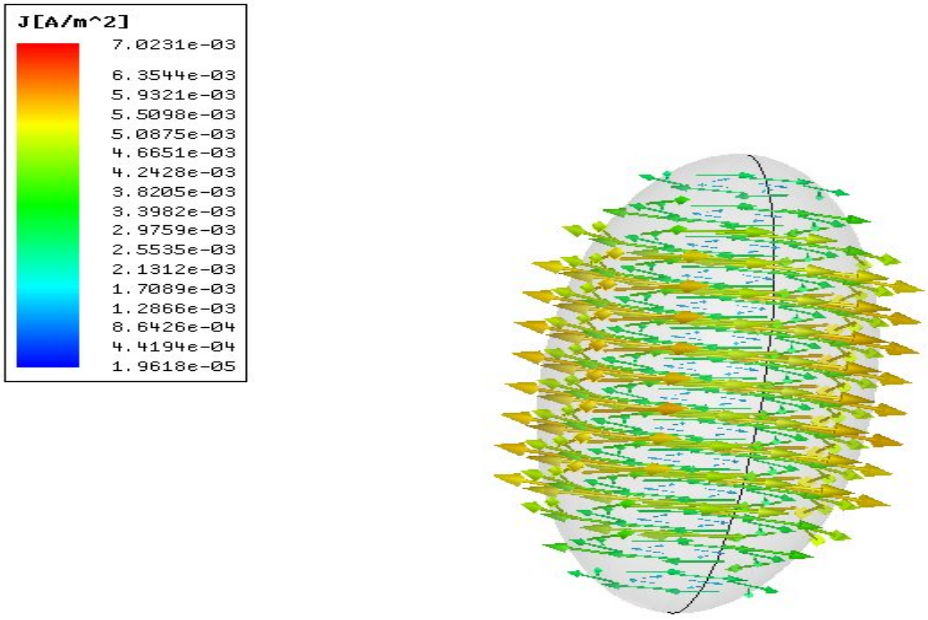

Figure 3 : example of calculation of induced currents in an ellipsoid with a fine mesh

Table 1 (resp. Table 2) summarizes results for a magnetic induction along z-axis and y-axis for three sizes of ellipsoid with a coarse mesh (resp. for a fine mesh). The reference is given by analytical solution. For each code or formulation the first column indicates the relative error [RS1]computed with all tetrahedral. The second column indicates the relative error computed only with the tetrahedral satisfying the geometrical criterion.

Table 1 : Results for a magnetic induction along z-axis and y-axis for three sizes of ellipsoid with a coarse mesh

Benchmark	Reference (mA/m^2)	Getfem++ φ-A (mA/m^2)		Code_Carmel A-V (mA/m^2)		Code_Carmel T-Omega (mA/m^2)		Maxwell3D (mA/m^2)	
		Not corr.	Corr	Not corr.	Corr.	Not corr.	Corr	Not corr.	Corr.
Bz 60 x 30 cm	3,332	3,6	3,6	3,332	3,246	3,811	3,811	9,97	3,65
Bz 120 x 60 cm	6,664	10,3	10.2	6,578	6,565	12,459	9,281	13,977	7,415
Bz 180 x 80 cm	8,886	15,1	13,5	8,8155	8,731	10,2478	10,2478	27,736	12,49
By 60 x 30 cm	5,331	7,5	6,1	8,285	5,29	5,457	5,457	4,868	3,4
By 120 x 60 cm	10,662	18,2	14,6	23,469	11,415	12,1408	12,1408	19,719	14,748
By 180 x 80 cm	14,84	24,7	16,1	46,99	15,302	9,52	8,23	29,026	15,982

Table 2 : Results for a magnetic induction along z-axis and y-axis for three sizes of ellipsoid with a fine mesh

Benchmark	Reference (mA/m^2)	Getfem++ φ-A (mA/m^2)		Code_Carmel A-V (mA/m^2)		Code_Carmel T-Omega (mA/m^2)		Maxwell3D (mA/m^2)	
		Not corr.	Corr	Not corr.	Corr	Not corr.	Corr	Not corr.	Corr
Bz 60 x 30 cm	3,332	3,6	3,6	3,291	3,291	3,326	3,326	3,326	3,326
Bz 120 x 60 cm	6,683	7,1	7,1	6,579	6,579	6,683	6,683	6,6834	6,6834
Bz 180 x 80 cm	8,886	9,5	9,5	8,785	8,785	8,904	8,904	8,904	8,904
By 60 x 30 cm	5,331	5,3	5,3	5,302	5,302	5,175	5,175	5,175	5,175
By 120 x 60 cm	10,662	10,4	10,4	10,652	10,652	10,407	10,407	10,387	10,387
By 180 x 80 cm	14,84	14,9	14,9	14,761	14,761	14,528	14,528	14,5	14,5

As mentionned above, the criterion for the mesh quality is fixed to 10%. As we can show in figure 4, this criterion filter lots of elements on the coarse mesh and few elements on the fine mesh.

Figure 4 : "bad elements" on the coarse and the fine mesh (in red)

DISCUSSION

Usually a finite element software user knows when the mesh is not fine enough. For instance, in figure 5, it is rather obvious that results on the left are not as good as those on the right. In such a simple case as the ellipsoids, a visual inspection may be sufficient. But when modelling a human phantom more accurate criteria are required.

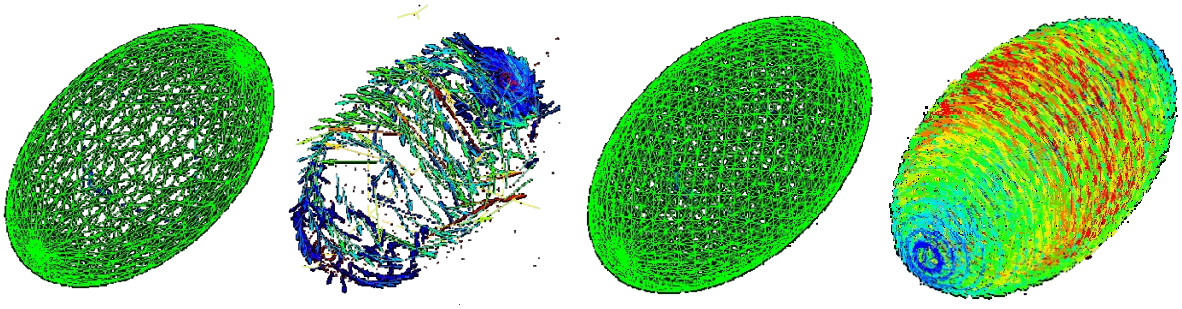

Figure 5: Induced current computation (coarse mesh – fine mesh)

The geometrical criterion on tetrahedron is a first step to evaluate the mesh quality. We can notice that with a fine mesh results are very close to the reference and no element was suppressed for post-processing.

With the coarse mesh results are heavily formulation dependant.

CONCLUSIONS

Results on a simple benchmark illustrate that the interest of filtering bad elements is twofold: on one hand, it allows achieving an improved accuracy with a moderate number of elements. On the other hand, it is useful to assess the robustness and the reliability of computations, in that large variations on the results obtained with or without filtering elements indicates a poor quality result. Both these points are very important when computing by using an anatomical phantom of the human body, because in practice it will lead to a huge mesh and then a huge problem to numerically solve.

BIBLIOGRAPHY

[1] Directive 2004/40/EC of the European Parliament and of the Council of 29 April 2004 on the minimum health and safety requirements regarding the exposure of workers to the risks arising from physical agents (electromagnetic fields). (Official Journal of the European Union, 29 April 2004).

[2] P. Dimbylow, "Current densities in a 2 mm resolution anatomically realistic model of the body induced by low frequency electric fields", *Phys. Med. Biol.* **45** (2000) 1013-1022.

[3] P. Dimbylow, "Induced current densities from low-frequency magnetic fields in a 2 mm resolution, anatomically realistic model of the body", *Phys. Med. Biol.* **43** (1998) 221-230.

[4] R. Scorretti, N. Burais, O. Fabregue, A. Nicolas, L. Nicolas "Computation of the induced current density in to the human body due to relative LF magnetic field generated by realistic devices", *IEEE Trans. Mag.*, vol. 40, no. 2 (2004), pp 643-646.

[5] EN50392:2004, "Generic standards to demonstrate the compliance of electronic and electrical apparatus with the basic restrictions related to human exposure to electromagnetic fields" (2004).

[6] F.-X. Zgainski, "An a priori Indicator of Tetrahedron Finite Element Quality based on the Condition number of the Elementary Matrix", Conference on Electromagnetic Field Computation, Tucson (1998).

[7] K. Caputa, P.J. Dimbylow, T.W. Dawson, M.A. Stuchly, "Modelling fields induced in humans by 50/60 Hz magnetic fields: reliability of the results and effects of model variations", *Phys. Med. Biol.* **47** (2002), 1391-1398.

[8] R. Cech, N. Leitgeb, M. Pediaditis, "Fetal exposude to low frequency electric and magnetic fields", *Phys. Med. Biol.* **52** (2007) 879-888.

[9] M. Sekino, S. Ueno, "FEM-based determination of optimum current distribution in transcranial magnetic stimulation as an alternative to electroconvulsive therapy", *IEEE Trans. Mag.*, vol 40, no 4, July 2004.

[10] O.P. Gandhi, G.Kang, D. Wu, G. Lazzi, "Currents induced in anatomic models of the human for uniform and nonuniform power frequency magnetic fields", *Bioelectromagnetics* **22** : 112-121 (2001).

[11] T.W. Dawson, K. Caputa, M.A. Stuchly, "Magnetic field exposures for UK live-line workers", *Phys. Med. Biol.* **47** (2002) 995-1012.

[12] C.M. Furse, O.P. Gandhi, "Calculation of electric fields and currents induced in a millimeter-resolution human model at 60 Hz using the FDTD method", *Bioelectromagnetics* **19**:293–299 (1998).

[13] A. Barchanski, T. Steiner, H. De Gersem, M. Clemens, T. Weiland, "Local grid refinement for low-frequency current computations in 3-D human anatomy models", *IEEE Trans. on Mag.*, vol. 42, no. 4, April 2006, 1371-1374.

[14] A. Barchanski, *Simulations of low-frequency electromagnetic fields in the human body*, PhD Thesis, Technischen Universität Darmstadt, 2007

[15] R. Scorretti, N. Burais, L. Nicolas, A. Nicolas, "Modeling of induced current into the human body by low-frequency magnetic field from experimental data", *IEEE Trans. on Mag.*, vol. 41, no. 5, May 2005, 1992-1995.

[16] L.H. Hoang, *Contribution à la modélisation tridimensionnelle des interactions champ électromagnétique-corps humain en basses fréquences*, PhD thesis, Ecole Centrale de Lyon, E.C.L.2007-32, (2007) pp. 53-57, 70-74, available on line at : http://tel.archives-ouvertes.fr/tel-00203230/en/.

[17] T. Henneron, Y. Le Menach, F. Piriou, O. Moreau, S. Clénet, J-P. Ducreux, J.-C. Vérité, "Source Field Computation in NDT applications", *IEEE Trans. on Mag.*, Vol.43, N°4, pp 1785-1788, 2007.

[18] GetFem++ : a finite element library, available on line at : http://home.gna.org/getfem/.